Materials Science & Engineering C 105 (2019) 110107

Contents lists available at ScienceDirect

Materials Science & Engineering C

journal homepage: www.elsevier.com/locate/msec

pH-responsive stearic acid-*O*-carboxymethyl chitosan assemblies as carriers delivering small molecular drug for chemotherapy

Fanghong Luo[a,b,c,1], Zhongxiong Fan[b,1], Wen Yin[d], Liu Yang[a], Tingting Li[a], Lubin Zhong[e], Yang Li[f], Shengyu Wang[a], Jianghua Yan[a], Zhenqing Hou[b,*], Qiqing Zhang[b,g,**]

[a] Cancer Research Center, Medical College, Xiamen University, Xiamen 361005, China
[b] Department of Biomaterials and Research Center of Biochemical Engineering, College of Materials, Xiamen University, Xiamen 361005, China
[c] Department of Chemistry, College of Chemistry and Chemical Engineering, Xiamen University, Xiamen 361005, China
[d] Lanzhou University Second Hospital, Lanzhou 730000, China
[e] Institute of Urban Environment, Chinese Academy of Sciences, 1799 Jimei Road, Xiamen 361021, China
[f] CAS Key Laboratory of Design and Assembly of Functional Nanostructures, and Fujian Provincial Key Laboratory of Nanomaterials, Fujian Institute of Research on the Structure of Matter, Chinese Academy of Sciences, Fuzhou 350002, China
[g] Institute of Biomedical Engineering, Chinese Academy of Medical Science and Peking Union Medical College, Tianjin 300192, China

ARTICLE INFO

Keywords:
Stearic acid-*O*-carboxymethyl chitosan assemblies
pH response
Small molecular drug
On-demand drug release
Cancer therapy

ABSTRACT

Recently, chemotherapy is still widely exploited to treat the residual, infiltrative tumor cells after surgical resection. However, many anticancer drugs are limited in clinical application due to their poor water-solubility (hydrophibic) and stability, low bioavailability, and unfavorable pharmacokinetics. Herein, an amphiphilic stearic acid-*O*-carboxymethyl chitosan (SA-CMC) conjugate was synthesized by amide linkage of SA to the backbone of CMC polymer and then self-assembled into nanoparticles (SA-CMC NPs) with the hydrodynamic particle size of ~100 nm. Subsequently, Paclitaxel (PTX) as a potent and broad-spectrum anticancer drug was loaded into SA-CMC NPs by a probe sonication combined with dialysis method. Owing to the multi-hydrophobic inner cores, the prepared PTX-SA-CMC NPs showed a considerable drug-loading capacity of ~19 wt% and a biphasic release behavior with an accumulative release amount in the range of 70–90% within 72 h. PTX-SA-CMC NPs remarkably enhanced the accumulation at the tumor sites by passive targeting followed by cellular endocytosis. Upon the stimuli of acid, PTX-SA-CMC NPs showed exceptional instability by pH change, thereby triggering the rapid disassembly and accelerated drug release. Consequently, compared with Cremophor EL-based free PTX treatment, PTX-SA-CMC NPs under pH-stimuli accomplished highly efficient apoptosis in cancer cells and effectively suppression of tumors by chemotherapy. Overall, PTX-SA-CMC NPs integrating imaging capacity might be a simple yet feasible PTX nanosystem for tumor-targeted delivery and cancer therapy.

1. Introduction

Cancer is still the leading cause of human death in the world, and conquering malignant tumors is a major challenge that mankind is facing [1]. Chemotherapy, one of the most universal methods for cancer treatments, often results in severely systemic side effects attributing to unspecific drug delivery to all organs and tissues including healthy ones [2]. Besides, the majority of anticancer drugs with potential bioactivity are seriously limited in clinical application due to the poor water-solubility and stability, fast degradation, short blood circulation, severe multidrug resistance MDR, rapid clearance, non-specific bio-distribution, low tumor accumulation, and undesired systemic toxicity [2,3]. Fortunately, the rapid developments of nanotechnology in the past few decades supply an innovative platform for prolonging the lifetime and life quality of cancer patients due to their significant biodistribution and bioavailability [4,5]. A rich variety of nano-carriers such as liposomes [6,7], polymeric micelles [8–10], protein based nanoparticles [11], polymer/drug-drug conjugates [12,13], inorganic nanoparticles [14,15], dendrimers [16], carbon nanotubes [17], and quantum dots [18,19] have been successfully developed for delivery hydrophobic

* Corresponding author.
** Correspondence to: Q. Zhang, Department of Biomaterials and Research Center of Biochemical Engineering, College of Materials, Xiamen University, Xiamen 361005, China.
E-mail addresses: houzhenqing@xmu.edu.cn (Z. Hou), zhangqiq@126.com (Q. Zhang).
[1] Contributed equally to this work.

https://doi.org/10.1016/j.msec.2019.110107
Received 19 January 2019; Received in revised form 5 August 2019; Accepted 20 August 2019
Available online 21 August 2019

drug to tumor tissue *via* passive (enhanced permeability and retention (EPR) effect mediated passive targeting effect) or active (ligand mediated active targeting effect) targeting [20,21]. Although these nanocarriers can remarkably enhance the pharmacokinetics and bio-distribution of anticancer drugs, they are largely limited by poor biocompatibility and the presence of a number of nonactive excipients might result in the undesired side effects [17].

Additionally, the polymeric nanoparticles self-assembled by amphiphilic conjugates in water solution, as a variety of nanomedicine delivery systems, have attracted wide attentions over the years [22]. Since the hydrophobic cores of the polymeric nanoparticles are surrounded *via* the hydrophilic outer shells. Therefore, the inner core can be regarded as a nano-container to load the hydrophobic anticancer drugs. Moreover, the circulation lifetime of intravenously injected nanoparticles can be relatively prolonged owing to the limited uptake *via* liver and spleen [22,23]. As the prolonged circulation lifetime of nanoparticles allows them to accumulate and extravasate at the tumor site by EPR effect, the reduced uptake by liver and spleen has been used for the treatment of solid tumors [23]. Overall, nanomedicine delivery systems based on the polymeric nanoparticles are effective strategy for passive tumor targeting with long retention time in the bloodstream.

Paclitaxel (PTX) as one of the most effective anticancer drugs has been widely used in the clinical treatment of various forms of cancer, including ovarian and breast cancer, nonsmall cell lung carcinoma, melanoma, head and neck cancer, AIDS-related Kaposi's sarcoma, and others [24,25]. PTX is an effective promoter of microtubulin polymerization which results in cell apoptosis *via* disturbing the dynamics of cell divisions. However, the high hydrophobicity of PTX (water solubility 0.3 μg/mL) hampers its clinical applications. To improve its water solubility, it is usually formulated with Cremophor EL in the clinical applications. Unfortunately, the application of Cremophor EL is related in the hypersensitivity reactions, neurotoxicity, and nephrotoxicity in up to 30% of the patients, and plasticizers can be extracted from intravenous infusion lines [26]. To address the problem, the development of alternative formulations without the application of other harmful excipients and organic solvents has drawn much attention from researchers.

Among the polysaccharides, chitosan possesses many excellent properties, such as biocompatibility, biodegradability, bioadhesivity, and non-toxicity that make it suitable as a nano biomedical material. Nonetheless, chitosan without amphiphilicity could not form nanomicelle. In the past decades, chitosan-based micellar system has been developed *via* grafting hydrophobic groups to the chitosan backbone and then used as the delivery carriers for genes [27], peptides [28], and antitumor drugs [29]. The chitosan-based amphiphilicity can form micelles by self-assembly in water solution.

In our previous study, SA as an endogenous long-chain saturated fatty acid has excellent biocompatibility and low toxicity, and is available for pharmaceutical use. The CMC hydropholic polymer was conjugated with SA successively *via* chemical coupling. Subsequently, PTX as a model anticancer drug was successfully encapsulated within SA-CMC NPs. These newly developed nanomedicine delivery systems could be expected to enhance the targeting and therapeutic effect greatly (Scheme 1c). The physicochemical characterization, *in vitro* drug release, *in vitro* cytotoxicity, *in vitro* cellular uptake, *in vivo* passive targeting effect and biodistribution, and *in vivo* antitumor efficiency of the advanced PTX-SA-CMC NPs were researched in detail.

2. Materials and methods

Paclitaxel (PTX, purity grade > 99%) was purchased from Tianfeng Biological engineering Co., Ltd., Shenyang, China. *O*-carboxymethyl chitosan (CMC, MW = 3.5 × 105, degree of deacetylatio n = 85.2%) was provided by Honghai biochemistry Co., Ltd., Qingdao, China. Stearic acid (SA) was purchased from Chemical Reagent Co., Ltd., Shanghai, China. The near-infrared (NIR) dye, Cy5.5 was purchased from PE Company, USA. Hoechst 33258 were provided by Invitrogen (USA). 1-Ethyl-3-(3-dimethylaminopropyl) carbodiimide (EDC), N-hydroxysuccinimide (NHS), 3-(4, 5-dimethylthiazol-2-yl)-2, 5-diphenyltetrazolium bromide (MTT), and 2, 4, 6-trinitrobenzene sulfonic acid (TNBS) were obtained from Sigma Chemical Co., Ltd., St. Louis, USA. BEL-7402 human liver cancer cell lines were obtained from Cancer Research Center, Medical College, Xiamen University. Dulbecco's minimum essential medium (DMEM) was obtained from GE Healthcare Life Sciences HyClone Laboratories. RPMI-1640, penicillin-streptomycin, and tryposin were obtained from Gibco BRL, USA. Pyrene was purchased from Aldrich Chemical Co., Ltd., USA, was purified by double recrystallization from absolute ethanol. Sodium salicylate was supplied by Wulian Chemical plant, China. Fetal bovine serum (FBS) was supplied by Sijiqing Biologic, China. The dialysis bags (MWCO = 3500 and 7000 DA) were from Spectrum Laboratories, USA. All other chemicals and reagents were analytical or chromatographic grade unless otherwise noted. All experiments were performed in compliance with the relevant laws and institutional guidelines. The experiments were carried out in accordance with the guidelines issued by the Ethical Committee of Xiamen University.

2.1. Synthesis of SA-CMC conjugate

The amphiphilic SA-CMC conjugate was synthesized *via* chemical conjugation of CMC with SA in the presence of EDC. Briefly, in a typical reaction, CMC (1.0 g) was dissolved in 30 mL of ultrapure water. SA (0.4 g) and EDC (0.81 g) were dissolved in 20 mL of ethanol by sonication treatment (JY92-II, Kunshan Ultrasonic Instrument Co. Ltd., Jiangshu, China) in the water bath. Subsequently, CMC solution was added to the mixture under magnetic stirring at 400 rpm. The reaction mixture was carried on stirring at 80 °C for 6 h and then cooled to room temperature. The reaction mixture was stirred sequentially for an additional 24 h. The prepared product was dialyzed against ultrapure water using dialysis membrane (MWCO 7 kDa) for 48 h to completely remove other water-soluble byproducts and then dried in a vacuum oven. The dried product was dispersed in 20 mL of ethanol and then treated with sonication to completely remove the un-reacted SA. The sonication step was repeated two times. The obtained suspension was filtered to collect the precipitate through 0.45 μm millipore filter. The precipitate was then dried, and the final product of SA-CMC conjugate was received.

2.2. Characterizations of SA-CMC conjugate

The Fourier transform infrared spectroscopy (FT-IR) spectra of CMC and SA-CMC conjugate powder were analyzed using Nicolet Avatar 380 Fourie Transfer Infrared Spectrometer

Next, ^{1}H nuclear magnetic resonance (NMR) spectra of CMC and SA-CMC conjugate were analyzed on a NMR Spectrometer (400 Hz, Bruker, Switzerland). CMC and SA-CMC conjugate was dissolved in D_2O solution.

2.3. Determination of the degrees of substitution (DS)

DS, referred to the SA per 100 sugar residues of CMC, was measured *via* TNBS method. Briefly, 20 mg of SA-CMC conjugate was dissolved in 20 mL of ultrapure water. Subsequently, 4 mL of SA-CMC conjugate solution was added to 4 mL of 4% $NaHCO_3$ and 4 mL of 0.1% TNBS at 40 °C for 1.5 h. 2 mL of HCl (2 N) was supplemented sequentially. The UV absorbance at 344 nm of the product against a blank was prepared with sodium hydrogen carbonate solution, TNBS solution, and ultrapure water under the same process, and determined *via* UV spectrophotometer (HELIOS ALPHA, Varian Instrument, USA). The amount of SA substitution was calculated by a calibration curve acquired *via* the amino-group measurement of a series of solutions with increasing the amount of CMC.

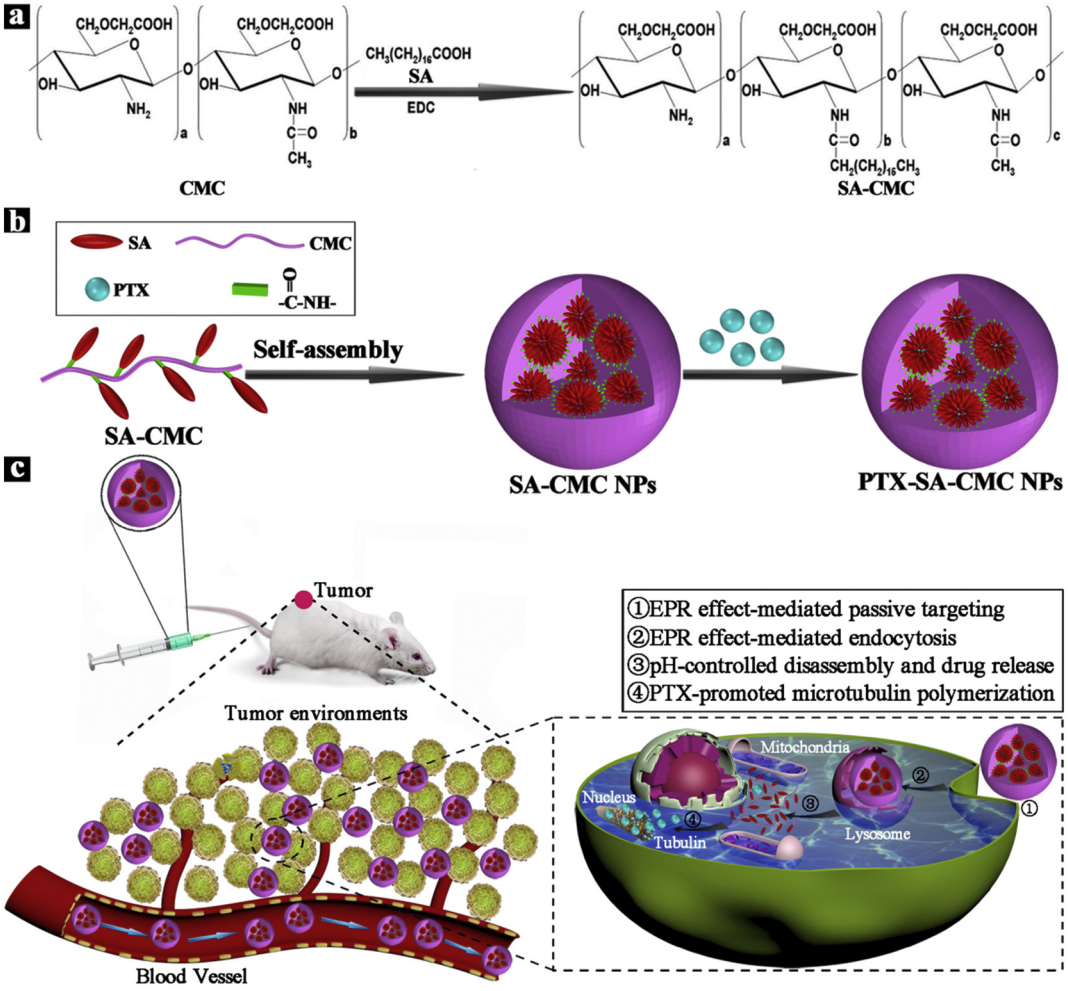

Scheme 1. (a) Synthetic route of SA-CMC. The SA-CMC conjugate was synthesized *via* the chemical coupling between carboxyl group of SA molecule and the amino group of CMC molecule, subsequently (b) Illustration of the self-assembly of PTX-SA-CMC NPs. (c) Schematic of drug delivery of PTX-SA-CMC NPs. Through the EPR effect-mediated passive targeting and the cellular endocytosis, PTX-SA-CMC NPs realized preferential tumor accumulation, pH-responsive drug release, and highly effectively chemotherapy after intravenous injection.

2.4. Determination of critical aggregation concentration (CAC)

To measure the self-aggregation behavior of SA-CMC conjugate and its CAC value, the pyrene as a fluorescence probe was used in our previous study. In brief, 6 mg of pyrene was dissolved in 50 mL of acetone to prepare the pyrene stock solution. Subsequently, the prepared pyrene stock solution was diluted with acetone for an additional 100 times. Exact 0.5 mL aliquots of pyrene solution at a concentration of 0.0012 mg/mL were precisely transferred into test tubes and then the solvent was evaporated in dark at 50 °C. 5 mL of SA-CMC conjugate solution at concentrations ranging from 1.0 mg/mL to 10^{-4} mg/mL was added to test tubes. The final concentration of pyrene in mixtures was controlled at 10^{-7} M. The emission spectra of mixture were determined by using fluorometer (LS-55, PE Co., Ltd., USA) (excitation wavelength of 335 nm).

2.5. Preparation of SA-CMC NPs and PTX-SA-CMC NPs

The amphiphilic SA-CMC conjugate was firstly self-assembled into SA-CMC NPs by probe sonication method in aqueous solution. In brief, SA-CMC conjugate was dispersed in ultrapure water under gentle shaking at 25 °C for 12 h, followed by sonication exploiting a probe type sonifier (Kunshan Ultrasonic Instrument Co. Ltd., Jiangshu, China) at 60 W for 2 min in an ice bath. The sonication step was repeated five times. The sample solution was filtered through 0.45 μm millipore filter to completely remove dust.

Next, the probe sonication-dialysis method was used to prepare PTX-SA-CMC NPs. Briefly, predetermined PTX (0.6–1.8 mg) were dissolved in methanol, and then the self-assembled SA-CMC NPs dispersion were slowly added under stirring followed by sonication using a probe type sonifier in an ice bath. Subsequently, to obtain the PTX-loaded self-assembled SA-CMC NPs, the residual methanol solvent was removed by dialysis (Millipore dialysis tube, MWCO, 14 kDa, USA). The impurity and dust in the PTX-loaded self-assembled SA-CMC NPs solution were removed by passing through 0.45 μm millipore filter, followed by lyophilization.

2.6. Characterizations of SA-CMC NPs and PTX-SA-CMC NPs

The samples for the transmission electron microscope (TEM, JEM2100, Japan) observation were prepared by dropping a solution of SA-CMC NPs and PTX-SA-CMC NPs onto a 300-mesh copper grid coated with carbon. The sample grid was allowed to dry completely at 25 °C. Observation was performed at 80 kV.

Next, the hydrodynamic diameter and zeta potential of SA-CMC NPs and PTX-SA-CMC NPs were determined *via* dynamic light scattering (DLS) and electrophoretic light scatterin (ELS) using a Malvern Zetasizer Nano-ZS (Malvern Instruments, Worcestershire, U.K.).

2.7. Drug-loading capacity and encapsulation efficiency

In this experiment, to measure the concentration of PTX in PTX-SA-CMC NPs, high performance liquid chromatography (HPLC, Agilent Technologies G171BA 1200 series, German) were used according to the following conditions: stationary phase, Diamohsil TM C18 column (250 mm × 4.6 mm, 5 μm); temperature, 25 °C; mobile phase, methanol: water (75:25, v/v), freshly prepared, filtered through a 0.22 mm Millipore membrane filter before using, and degassed by a sonication method; elution flow rate, 1 mL/min; detection wavelength, 227 nm. A calibration curve was used for quantification *via* calculating the PTX concentration of a dilution series of free PTX in PBS. Encapsulation efficiency and drug-loading content of PTX were calculated using the following formula [30]:

$$\text{PTX encapsulation efficiency } (\%) = \frac{\text{Weight}_{\text{PTX}} \text{ of Encapsulation}}{\text{Initial Weight}_{\text{Dox}}}$$

$$\text{PTX loading efficiency } (\%) = \frac{\text{Weight}_{\text{PTX}} \text{ of Encapsulation}}{\text{Initial Weight}_{\text{Tatal}}}$$

2.8. In vitro drug release of PTX-SA-CMC NPs

The *in vitro* release behavior of PTX from PTX-SA-CMC NPs was measured by dialysis technique using the cellulose ester membrane tube. A certain amount of PTX-SA-CMC NPs into a dialysis tube (MWCO 7 kDa) was immersed into 57 mL of phosphate-buffered saline (PBS) containing 0.1 M of sodium salicylate. The system was gently shaken under controlled condition at 37 °C in a water bath at 100 rpm. At a predesigned time point, 3 mL of the release medium was completely withdrawn and then replaced with the 3 mL of fresh PBS containing 0.1 M of sodium salicylate. The release amount of PTX was measured by UV–vis absorption spectroscopy. The cumulative release amount was calculated using the following formula.

$$\text{Cumulative release}(\%) = \frac{1 \times \sum_{i=1}^{n-1} \text{Ci} + 60 \times \text{Cn}}{\text{weight of drug in nanosystems}} \times 100\% \quad (2)$$

where Ci means the concentration of CUR drug in dialysate at i time.

2.9. Cell culture

BEL-7402 (human liver cancer) cell lines were cultured in RPMI-1640. BEL-7402 cell lines were obtained from Cancer Research Center, Medical College, Xiamen University and grew at the culture media supplemented with 10% FBS and 1% penicillin-streptomycin (100 U/mL). The cells were cultured in an incubator (Thermo Scientific) at 37 °C in a humidified atmosphere of 5% CO_2.

2.10. In vitro cytotoxicity of PTX-SA-CMC NPs

In vitro cytotoxicity was evaluated *via* MTT assay according to the manufacturer's suggested procedure. BEL-7402 cells were exposed to PTX-SA-CMC NPs with different PTX concentrations (0.01, 0.1, 1, and 10 μg/mL) for 48 h. The data was expressed by the percentage of the relative cell viability. Cremophor EL, Cremophor EL-based PTX and SA-CMC NPs were used as controls.

2.11. In vitro cellular uptake of PTX-SA-CMC NPs

To realize fluorescence labeling, Cy5.5-labeled PTX-SA-CMC NPs (Cy5.5-PTX-SA-CMC NPs) (14.9 wt%) were prepared as follows: 1 mg of Cy5.5-NHS was dissolved in 25 mL of anhydrous DMSO and then dropped into the SA-CMC conjugate solution (110 mg/40 mL) in anhydrous DMSO. The reaction mixture was stirred overnight at 25 °C and dialyzed against ultrapure water using a cellulose membrane (MWCO 7 kDa) for 2 d. The blue solution was lyophilized and blue powder (Cy5.5-PTX-SA-CMC NPs) was obtained. Lastly, Cy5.5-PTX-SA-CMC NPs were prepared by a probe sonication combined with dialysis method described as above.

Next, to visually trace the cellular uptake of PTX-SA-CMC NPs, the *in vitro* cellular uptake of Cy5.5-PTX-SA-CMC NPs was carried out by confocal laser scanning microscopy (CLSM). BEL-7402 cells were seeded into 6-well plates at a density of 1.0×10^4 cells per well, incubated at 37 °C for 24 h, and then treated with Cy5.5-PTX-SA-CMC NPs at regular time points (at 1, 3, 6, and 24 h) at 37 °C. After treatment, the cells were washed three times and then fixed by 4% paraformaldehyde for 3 min at 25 °C. Subsequently, the cells were washed with PBS and the nuclei were stained by Hoechst 33258 for 10 min. Finally, the cells were imaged using a Olympus FV1000 CLSM with excitation at 360 nm for Hoechst 33258 and 640 nm for Cy5.5.

2.12. In vivo biodistribution of PTX-SA-CMC NPs

All female athymic nude mice (6 weeks, female, 16–18 g) were provided by Shanghai SLAC Laboratory Animal CO, LTD. We subcutaneously injected BEL-7402 cells into the dorsal side of mice to establish BEL-7402 tumor-bearing models. Cy5.5-PTX-SA-CMC NPs were prepared by the method described as above for *in vivo* fluorescence imaging. When the tumor diameter was ~8 mm, physiological saline (100 μL) and Cy5.5-PTX-SA-CMC NPs (5 mg/kg in 100 μL of physiological saline) were intravenously injected *via* the tail vein into BEL-7402 tumor-bearing mice. The *in vivo* passive tumor targeting and imaging was observed at a predetermined point after injection using a MaestroTM *in vivo* imaging system (Cambridge Research and Instrumentation, Woburn, MA, USA).

Next, to provide a substantial evidence of the tumor specificity of PTX-SA-CMC NPs, *ex vivo* fluorescence imaging was further performed in BEL-7402 tumor-bearing mice. At 72 h post-injection, the Cy5.5-PTX-SA-CMC NPs-treated mice were sacrificed, and the tumor and major organs (tumor, liver, spleen, lung, kidney, and heart) were excised, followed by washing the surface with 0.9% NaCl. The resulting data were used to identify, separate, and remove the contribution of autofluorescence in analyzed images. All data were calculated by the region-of-interest (ROS) function of Analysis Workstation software (ART Advanced Research Technologies Inc., Montreal, Canada).

2.13. In vivo antitumor efficiency of PTX-SA-CMC NPs

The antitumor efficiency of PTX-SA-CMC NPs was evaluated in BEL-7402 liver tumor-bearing Kunming mice. We subcutaneously injected BEL-7402 liver cancer cells into the dorsal side of mice to establish BEL-7402 liver tumor-bearing models. When the tumor diameter was ~8 mm, these tumor-bearing mice (10 per group) were intravenously injected *via* the tail vein with Cremophor EL-based PTX, PTX-SA-CMC NPs (14.9 wt%), SA-CMC NPs alone, and physiological saline. Cremophor EL-based PTX and PTX-SA-CMC NPs were given at 0, 4, and 8 day so that the PTX dose would be 20 mg/kg (was the maximum tolerated dose). The tumor size was calculated by $a \times b^2/2$, where a represented the largest diameter and b represented the smallest diameter. The survivals of mice were also recorded.

3. Results and discussion

3.1. Synthesis and characterization of SA-CMC conjugate

CMC, a hydrophilic chitosan derivative, has two kinds of active groups, which can be functionalized by chemical coupling. One kind of them is hydroxyl group from C_6-OH and C_3-OH, the other kind is amino group. Generally, to endow CMC with some potential characteristics,

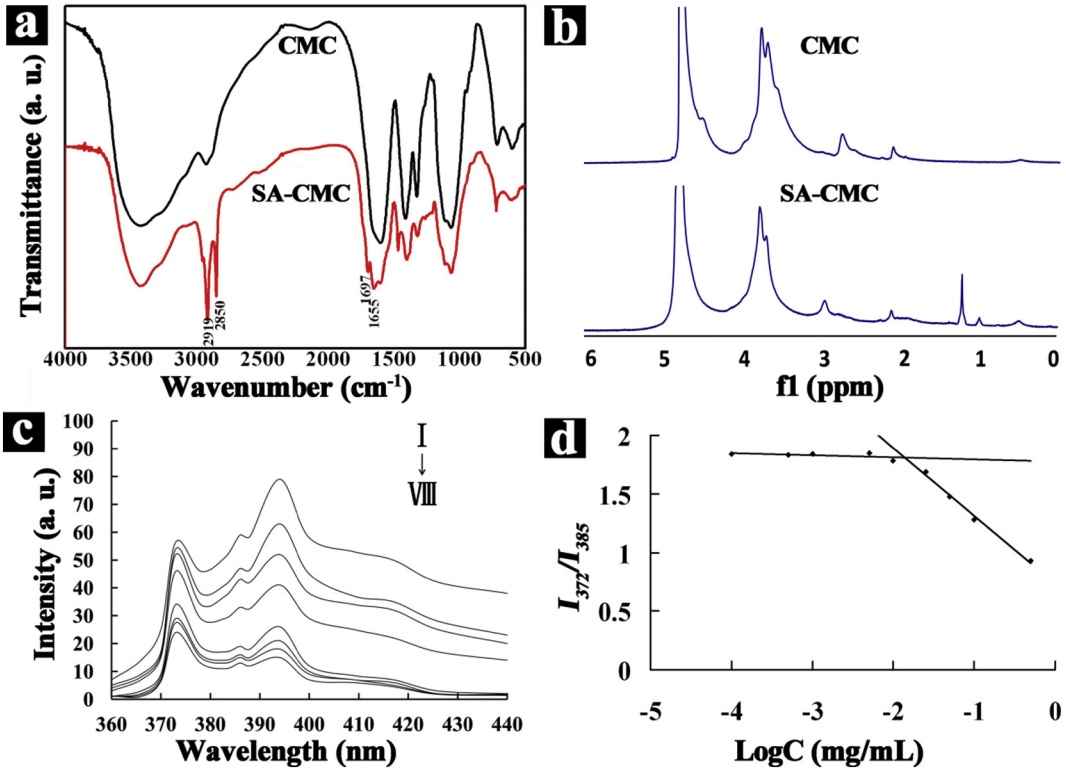

Fig. 1. (a) FTIR and (b) ^{1}H NMR spectra of CMC and SA-CMC conjugate. (c) The fluorescence emission spectra of pyrene (6.0×10^{-7} M) dissolved in an aqueous solution at 25 °C were affected by the different concentrations of SA-CMC co. (I) 1, (II) 0.1, (III) 0.05, (IV) 0.01, (V) 0.005, (VI) 0.001, (VII) 0.0005, and (VII) 0.0001 mg/mL. The spectra were accumulated with an integration time of 5 s/1 nm (excitation wavelength of 335 nm). (d) Intensity ratio (I_{372}/I_{385}) for pyrene in PBS (pH 7.2) and a function of the concentrations of SA-CMC.

peptide and alkyl are grafted to its molecule *via* coupling reaction. SA as an endogenous long-chain saturated fatty acid has excellent biocompatibility and low toxicity, and is available for pharmaceutical use. Therefore, the amphiphilic SA-CMC conjugate was first synthesized *via* an amine-reactive coupling reaction between the amino group of CMC molecular and the carboxyl group of SA molecular (Scheme 1a). In brief, EDC, a coupling cosslinker could be react with the carboxyl group of SA molecular and give an active intermediate-O-acylisourea derivation. Further addition of CMC including primary amino groups produced hydrophobically modified CMC amphiphiles *via* a stable amide. The resultant mixture was dialyzed against ultrapure water to remove by-product (isourea) and the remained EDC, and the excess of SA was washed by ethanol. Finally, the lyophilized SA-CMC conjugate could be easily dispersed in ultrapure water.

The chemical structure of CMC and SA-CMC was measured by FTIR and ^{1}H NMR analysis. As shown in Fig. 1a, the characteristic absorption peaks of CMC at 3419 cm^{-1}, 2929 cm^{-1}, 1601 cm^{-1}, 1411 cm^{-1}, 1325 cm^{-1}, and 1065 cm^{-1} could be ascribed to stretching vibration of the hydroxyl group, C—H stretching vibration, amide N—H bending, stretching vibration of hydroxyl group in the carboxyl group, the amide III stretching (C—N stretching vibration), and C—O stretching vibration, respectively. Moreover, our results were well consistent with some literatures [31,32]. In comparison with CMC, the characteristic absorption peaks of SA-CMC conjugate at 1697 $cm^{-1}$and 1655 cm-1 were relevant to the presence of the amide I stretching (C═O bending of the secondary amide) and the amide II stretching (N—H bending of the secondary amide), respectively. Besides, the characteristic absorption peaks at 2919 and 2850 cm^{-1} could be attributed to the asymmetric and symmetric C—H stretching modes of $–CH_2$ groups of SA, respectively. These results demonstrated that an amide linkage was formed between amino groups of CMC molecular and carboxyl groups of SA molecular.

Next, to further demonstrate the successful synthesis of SA-CMC conjugate, the ^{1}H NMR spectra of CMC and SA-CMC congjugate were shown in Fig. 1b. These proton signals of CMC at 2.10, 2.74, 3.77, 4.51, and 4.87 ppm could be attributed to CH_3 (acetamido group of chitosan), CH_2 (carboxymethyl group), CH (carbon 2 of glucosamine ring with the substituted amino group), CH (carbon 3, 4, 5 and 6 of glucosamine ring), and CH (carbon 1 of glucosamine ring). In comparison with CMC, the new proton signals of SA-CMC conjugate at 0.49, 0.98, and 1.19 ppm could be observed. The result indicated that SA was successfully linked to CMC.

Next, we measured the degree of DS *via* the TNBS method. DS, referred to the SA per 100 sugar residues of CMC, increased with increasing the feeding mole ratio of SA. A series of SA-CMC conjugates with different DS could be synthesized *via* controlling the feed ratio of SA and EDC to CMC. TNBS could react with the remained primary amino residues in SA-CMC conjugate. The DS of the SA-CMC conjugate was determined as ~13.8%.

3.2. Determination of critical aggregation concentration (CAC)

To measure the self-aggregation behavior of SA-CMC conjugate and its CAC value, the pyrene as a fluorescence probe was widely used [33]. Fig. 1c showed the fluorescence emission spectra of pyrene at different concentrations of SA-CMC in ultrapure water after sonication. The total fluorescence intensity of pyrene significantly increased with increasing the concentration of SA-CMC conjugate. The result implied that SA-CMC conjugate was aggregated to form hydrophibic micro-domains and the pyrene molecular was transferred from aqueous media into these micro-domains. Additionally, in the pyrene emission spectra, there were five vibrational peaks. The intensity ratio of the first peak at 372 nm and the third peak at 385 nm (I_{372}/I_{385}) was extremely sensitive to micro-environment. This could be attributed to the fact that

increasing the polarity of the medium induced an increase in the intensity of the first peak I_{372}, corresponding to the forbidden transition. On the contrary, the third the intensity of the third peak I_{385}, corresponding to the allowed transition, was not changed. Besides, the value of the intensity ratio was higher in the majority of polar media. [34] Thus the CAC value was the threshold concentration of self-aggregate formation *via* intramolecular or intermolecular association. Usually, the CAC value could be measured from the alteration of the I_{372}/I_{385}value of pyrene in the existence of polymeric amphiphiles.

Next, we studied the alterations of the I_{372}/I_{385} values as a function of the concentrations of SA-CMC conjugate. The I_{372}/I_{385} values were close to 1.87 of pyrene in PBS solution (pH 7.2) at low concentrations. Subseqently, with further increasing concentration, The I_{372}/I_{385} values showed a linear decrease (Fig. 1d). Thus the CAC value was tested as 0.0117 mg/mL *via* the intercept of two straight lines, which was much lower compared with that of the traditional surfactants such as sodium dodecyl sulfate in ultrapure water (2.3 mg/mL). [35] The stable SA-CMC NPs with lower CAC value could preserve their own structural stability in physiological condition during the circulation. However, in our previous study we found it was relatively difficult for CMC molecules to aggregate in the range of concentrations [36]. Therefore, It could be speculated that the aggregation degree of SA-CMC conjugate in water was attributed to the hydrophobic interactions of SA portions.

3.3. Preparation and characterizations of PTX-SA-CMC NPs

The amphiphilic SA-CMC conjugate was firstly self-assembled into SA-CMC NPs in aqueous environment. Subsequently, PTX as a hydrophobic anticancer drug molecular was physically encapsulated inside the SA-CMC NPs to form PTX-SA-CMC NPs. The morphology of the SA-CMC NPs and PTX-SA-CMC NPs was observed by TEM (Fig. 2a and b). TEM images clearly showed that the SA-CMC NPs and PTX-SA-CMC NPs were spherical shape, excellent aqueous dispersibility, and uniform diameter distribution. The mean diameter of PTX-SA-CMC NPs was slightly larger compared with that of SA-CMC NPs. Significant core-shell structure could be observed in PTX-SA-CMC NPs (Fig. 2c). More interestingly, PTX-SA-CMC NPs exhibited multi-core spherical characteristic when the TEM image was magnified from 5000 to 8000-fold (Fig. 2d). It could be deduced that the self-assembled SA-CMC NPs accord with multi-core model which was first brought forward by Akiyoshi et al. in 1997 [37]. The mechanism of formation of self-assembled SA-CMC NPs and PTX-SA-CMC NPs was shown in Scheme 1b, SA-CMC conjugate was composed by the hydrophilic carboxymethy of CMC and the hydrophobic portions of SA. In the aqueous phase, the amphiphilic SA-CMC conjugate was self-assembled into NPs, the hydrophobic cores of polymeric NPs were encircled with hydrophilic outer shells. Therefore, the inner core could be acted as a nano-container for accommodating the hydrophobic anticancer drugs, and PTX was entrapped into the inner cores by hydrophobic interactions between drug and core domain.

The amphiphilic SA-CMC conjugate formed SA-CMC NPs spontaneously in water solution (PBS or ultrapure water). Dynamic light scattering (DLS) demonstrated that SA-CMC NPs were of the mean hydrodynamic diameter of 138.2 nm, the polydispersity index (PDI) of 0.134, and the zeta potential of about −17.2 mV (Table 1). The average diameter of these NPs measured by TEM was ~98 nm which was smaller compared with the mean hydrodynamic diameter determined by DLS. This was mainly attributed to the process involved in preparation of samples. Therefore, due to solvent effect, the diameter measured by DLS was larger compared with that determined by TEM. In addition, the mean diameter of PTX-SA-CMC NPs was slightly larger than the SA-CMC NPs due to the entrapment of PTX drug into the inner cores, and the average diameter measured by TEM increased from 106 to 123 nm along with the increase of PTX drug-loading capacity. Therefore, we forecasted that the small size (about 100 nm), negative charge, favorable stability in biological condition may be suitable for the EPR effect at the site of a solid tumor [23,38]. Moreover, the size of PTX-SA-CMC NPs could not only make them ideal drug delivery system for delaying macrophage clearance in reticular endothelial system (RES), but also enhance their vascular permeability. These results indicated that PTX-SA-CMC NPs could exhibit a passive tumor targeting with long retention time in the bloodstream.

3.4. Drug-loading capacity and encapsulation efficiency

Drug-loading capacity, encapsulation efficiency, and their respective average diameter of PTX-SA-CMC NPs were listed in Table 1. With the feed-weight ratio of PTX adding from 10% to 30%, the PTX drug-loading capacity increased from 8.6% to 18.8%. Meanwhile, the PTX encapsulation efficiency reduced from 86.0% to 62.0%. Based on the diameter and the drug-loading characteristic, the optimal feed-weight (20%) ratio was chosen to prepare PTX-loaded SA-CMC NPs. The solubility of PTX in micellar systems self-assembled by the SA-CMC conjugatewas up to 1.86 mg/mL that was about 2000-fold higher compared with that of the saturated concentration of PTX in ultrapure water. The PTX-loading capacity was obviously greater compared with the other polysaccharide-based amphiphiles and SA-CMC NPs. [39,40] This higher drug-loading capacity of PTX-SA-CMC NPs was likely attributed to the presence of multi-hydrophobic inner cores.

3.5. In vitro drug release of PTX-SA-CMC NPs

Dialysis method was used to research the release profile of PTX from PTX-SA-CMC NPs. For *in vitro* release profiles of water-insoluble drugs like PTX, the choice of the medium is vital because such drugs are not easily released in the absence of detergents or organic solvents. Nevertheless, the traditional detergents or organic solvents frequently disintegrate the self-assembled NPs, which may have an influence on the release profile of PTX. In our previous work, to induce the release of PTX from the PTX-CA-CMC NPs, sodium salicylate was successfully exploited as the hydrophobic agent. [40] Thus, the *in vitro* release behavior of the self-assembled PTX-SA-CMC NPs was administered in PBS

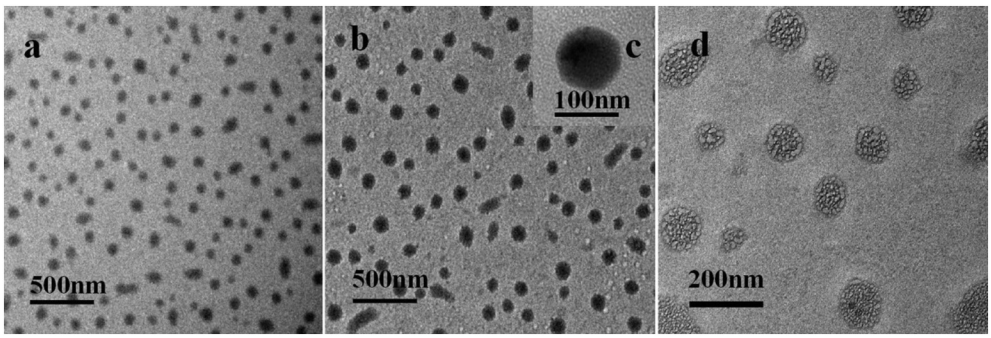

Fig. 2. TEM image of SA-CMC NPs (a, ×5000) and PTX-SA-CMC NPs (14.9%) (b, c, ×5000; d, ×8000) in ultrapure water (1 mg/mL).

Table 1
Characteristics of SA-CMC NPs and PTX-SA-CMC NPs.

Sample	Feed ratio of PTX/SA-CMC (%)	Loading capacity of PTX[a] (wt%)	Encapsulation efficiency of PTX[b] (%)	Mean diameters (nm)	PDI	Zeta potential (mV)
SA-CMC NPs	–	–	–	98 ± 11[c] 138.2 ± 21.3[d]	0.134 ± 0.012	−17.2
PTX-SA-CMC NPs (10 wt %)	10	8.6 ± 0.3	86.0 ± 4.3	106 ± 19[c] 145.8 ± 23.1[d]	0.225 ± 0.012	−23.2
PTX-SA-CMC NPs (20 wt %)	20	14.9 ± 0.5	74.5 ± 3.8	115 ± 13[c] 151.5 ± 29.6[d]	0.232 ± 0.015	−25.6
PTX-SA-CMC NPs (30 wt %)	30	18.8 ± 0.9	62.0 ± 2.9	123 ± 24[c] 157.6 ± 22.4[d]	0.185 ± 0.012	−27.8

[a] Loading capacity of PTX in SA-CMC NPs were measured *via* encapsulation.
[b] Encapsulation efficiency of PTX in SA-CMC NPs was calculated from the ratio of loading amount of PTX to feed amount of PTX in SA-CMC NPs.
[c] Average diameter of each n was measured using TEM.
[d] Average diameter of each particle (1 mg/mL in PBS) was measured *via* DLS.

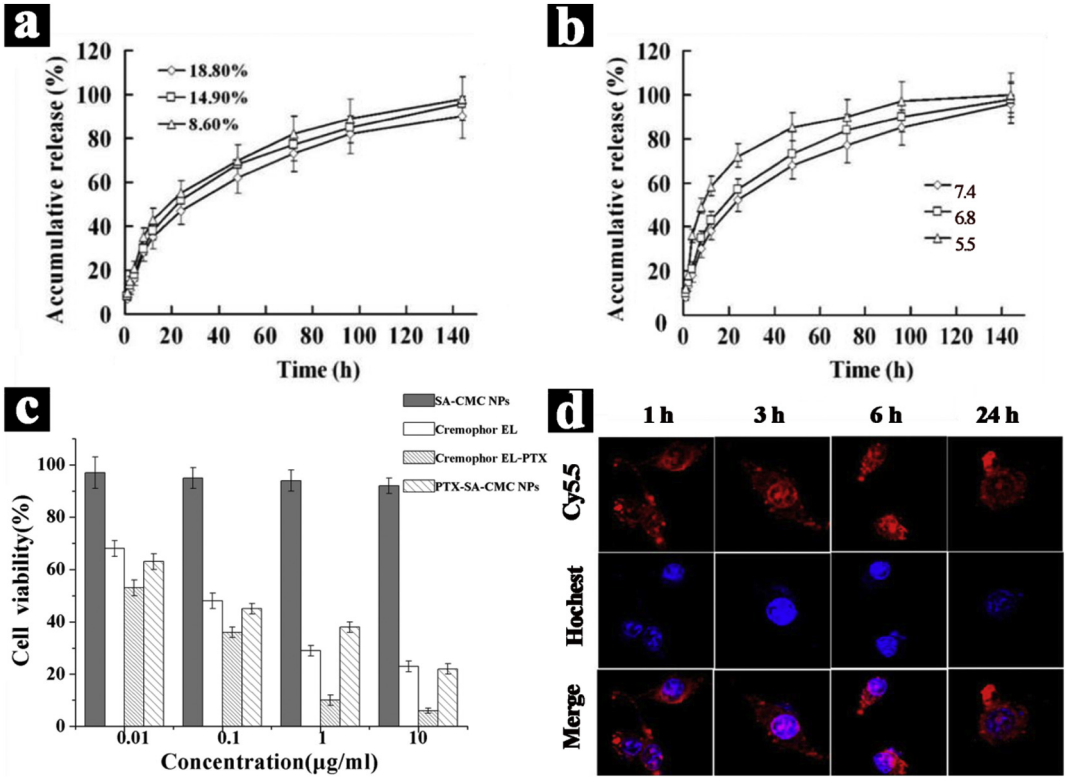

Fig. 3. (a) PTX release profiles from PTX-SA-CMC NPs with different drug-loading capacity at 37 °C in PBS with 0.1 M sodium salicylate. (b) PTX release profiles from PTX-SA-CMC NPs with drug-loading capacity of 14.9% at 37 °C in PBS comprising 0.1 M sodium salicylate with different pH value. Data represents mean ± s. d. (n = 3). (c) *In vitro* cytotoxicity of SA-CMC NPs and PTX-SA-CMC NPs (14.9 wt%) measured using MTT assay. Data represents mean ± s. d. (n = 5). (d) *In vitro* cellular uptake and intracellular drug delivery of Cy5.5-PTX-SA-CMC NPs (14.9 wt%). CLSM images of BEL-7402 cells incubated with Cy5.5-PTX-SA-CMC NPs (14.9 wt%) for 1, 3, 6, and 24 h incubation (original magnification, × 400). The cell nuclei were stained with Hoechst 33258. False-color Blue: Hoechst 33258. False-color red: Cy5.5. (For interpretation of the references to color in this figure legend, the reader is referred to the web version of this article.)

with 0.1 M sodium salicylate at 37 °C.

To measure the release profile of PTX from PTX-SA-CMC NPs with different PTX-loading content (8.60, 14.90, and 18.80 wt%, respectively), these PTX-SA-CMC NPs were dispersed in PBS with 0.1 M sodium salicylate, and then dialyzed at 37 °C for 140 h. As shown in Fig. 3a, the release of PTX from PTX-SA-CMC NPs (14.9 wt%) shown a biphasic stage. The initial stage was a burst release stage, which could be convenient for the inhibition of the tumor cell growth in a short time. And the subsequent stage was a sustained release stage, which could offer the probability of continually fighting against the tumor cell. Besides, the initial burst effect was observed within 12 h, in which nearly 40% of PTX was released from SA-CMC NPs. Subsequently, PTX was released in a continuous and sustained way for up to 140 h, reaching the cumulative release rate close to 96%. Therefore, the self-assembled SA-CMC NPs delayed the release process of PTX. The similar release characteristic was also observed in PTX-SA-CMC NPs with different loading capacity (8.60 and 18.80 wt%). However, the release rate decreased with the increase of PTX-loading capacity, probably due to the drug crystal formed in the inner cores when the drug concentration was relatively high.

In addition, to determine the release profile of PTX from PTX-SA-CMC NPs, they were dispersed in PBS comprising 0.1 M sodium salicylate with pH 7.4, 6.8, and 5.5, respectively, and then dialyzed at 37 °C for 140 h. AS exhibited in Fig. 3b, PTX-SA-CMC NPs showed significantly pH-dependent release behavior. Moreover, It could be found that PTX release from PTX-SA-CMC NPs was lower at pH 7.4 (about

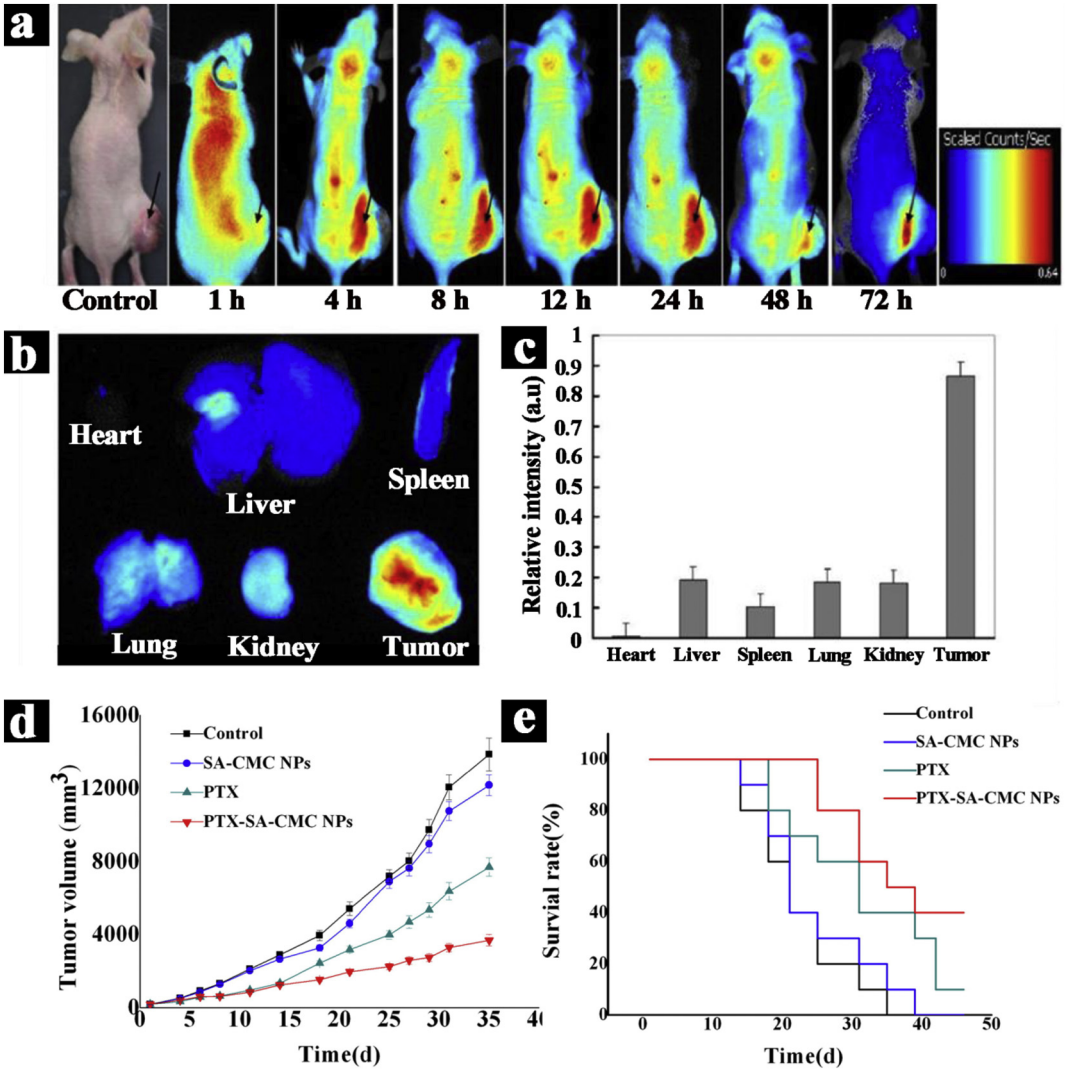

Fig. 4. (a) *In vivo* NIR fluorescence images of BEL-7402 tumor-bearing nude mice after intravenous injection of the Cy5.5-PTX-SA-CMC NPs for 1, 4, 8, 12, 24, 48, and 72 h. (b) *Ex vivo* NIR fluorescence images of normal organs and tumors dissected from BEL-7404 tumor-bearing nude mice at 72 h post-injection of Cy5.5-PTX-SA-CMC NPs. (c) Mean fluorescence signals of the dissected organs and tumors at 30 h post-injection. (d and e) *In vivo* antitumor efficiency of BEL-7402 liver tumor-bearing nude mice after intravenous injection of physiological saline, Cremophor EL-based PTX, SA-CMC NPs, and PTX-SA-CMC NPs (14.9 wt%). (d) Relative Tumor volume. (e) The survival rate. Tumor sizes were measured every 2–3 days. Data represents mean ± s. d. (n = 10).

65%) than at pH 5.0 (nearly 85%) at 48 h. This pH-dependent PTX release could be ascribed to the increased PTX solubility and weakened interactions between the PTX and SA-CMC conjugate under acidic conditions. This release manner might be advantageous to controlled and sustained drug release. The results indicated PTX-SA-CMC NPs could maintain a relatively slower release rate in the blood circulation with neutral pH, and turn to a relatively faster release rate in the mildly acidic tumor tissue and significantly acidic endo/lysosomes inside tumor cells. Notably, the accumulative release rate was in range of 73–90% within 72 h. the result implied that PTX-SA-CMC NPs could maintain drug release in a long period. It might be a great improvement to SA-grafted chitosan oligosaccharide self-assembled micelles.

3.6. In vitro cytotoxicity of PTX-SA-CMC NPs (14.9 wt%)

To explain the cell-killing effect of PTX-SA-CMC NPs, BEL-7402 human liver cancer cells were treated with the Cremophor EL, Cremophor EL-based PTX, SA-CMC NPs, and PTX-SA-CMC NPs. The cell viability was evaluated using MTT assay. As shown in Fig. 3c, PTX-SA-CMC NPs exhibited obviously concentration-dependent cytotoxicity. Moreover, PTX-SA-CMC NPs exerted some extent of cancer cell-killing effect, BEL-7402 cells treated with PTX-SA-CMC NPs retained higher viabilities than those exposed to Cremophor EL-based PTX. The result could be ascribed to the fact that Cremophor EL enhanced the cytotoxicity of free PTX. It was also explained that the cytotoxic PTX molecules were released from PTX-SA-CMC NPs in a sustained and prolonged manner, resulting in a reduced cytotoxicity compared with free PTX in a relatively short time. Besides, when BEL-7402 cells were treated with SA-CMC NPs at various concentrations used in this study, the majority of cells were viable and cell viability remained above 96%. The result implied that the empty SA-CMC NPs (was exactly safe and biodegradable) had little cytotoxicity against BEL-7402 cells. As a main composition of fat, SA was biocompatible with low toxicity. It was also reported that CMC showed excellent biocompatibility. [36,41] In a word, the cytotoxicity of PTX-SA-CMC NPs was resulted in the released PTX but not was induced by SA-CMC NPs. Therefore, PTX-SA-CMC NPs might have potential as an effective and safe drug carrier for cancer therapy.

3.7. In vitro cellular uptake of PTX-SA-CMC NPs (14.9 wt%)

To track the cellular uptake of PTX-SA-CMC NPs, Cy5.5 as a

fluorescence probe was used to label the CMC backbone by coupling NHS ester group of Cy5.5 and amine groups of CMC *via* stable amide linkage. BEL-7402 human liver cancer cells were incubated with Cy5.5-PTX-SA-CMC NPs at a fixed PTX concentration of 10 μg/mL for 1, 3, 6, and 24 h at 37 °C and observed using the confocal laser microscopy. Hoechst 33258 was used to identify the cell nuclei. As shown in Fig. 3d, the Cy5.5-PTX-SA-CMC NPs (red fluorescence) were readily taken up *via* BEL-7402 cells after 1 h incubation, and were evenly distributed in the cytoplasm or around the nucleus (blue fluorescence). After 3 and 6 h incubation, the stronger red fluorescence signal was clearly observed inside BEL-7402 cells than that after 1 h incubation. CLSM results implied that cellular uptake of PTX-SA-CMC NPs was in an endocytosis manner. Besides, studies have shown that cellular uptake of the free PTX was in a passive diffusion way. [42] This result indicated that PTX-SA-CMC NPs might be internalized by BEL-7402 cells, in which the higher amount of PTX could be delivered into the cytoplasm to induce cell death.

3.8. *In vivo* passive targeting effect and biodistribution of PTX-SA-CMC NPs (14.9 wt%)

To investigate the *in vivo* tumor passive targeting effect of PTX-SA-CMC NPs (14.9 wt%), the time-dependent biodistribution was examined by noninvasive NIR imaging technique. The NIR fluorescence probe Cy5.5-PTX-SA-CMC NPs were administrated into BEL-7402 tumor-bearing mice by intravenous injection. As shown in Fig. 4a, the *in vivo* fluorescence imaging indicated that the fluorescent signals of PTX-SA-CMC NPs were distributed in the whole body within 1 h post-injection, indicating the rapid circulation of NPs in the blood stream. Notably, the Cy5.5-PTX-SA-CMC NPs were mainly localized at the tumor sites (Black arrows indicate the tumor site) at 4 h post-injection. Moreover, the fluorescence signals at the tumor site continued to increase up to 24 h post-injection and maintained up to 24 h. The result suggested that the Cy5.5-PTX-SA-CMC NPs could escape the reticuloendothelial systems (RES) and efficiently accumulate in the tumor tissue. In our opinion, the result could probably be attributed to the EPR effect-mediated passive tumor specificity of PTX-SA-CMC NPs. In addition, although the strong NIR fluorescence signal in the whole body gradually decreased after 24 h and almost disappeared till 72 h, the obvious NIR fluorescence signal was still accumulated at the areas of tumor tissue. In a word, the results indicated that the Cy5.5-PTX-SA-CMC NPs exhibited excellent passive tumor targeting efficiency.

To provide a substantial evidence of the tumor specificity of PTX-SA-CMC NPs, major organs and tissues (heart, liver, spleen, lung, kidney, and tumor tissues) were dissected from BEL-7402 tumor-bearing mice at 72 h after intravenous injection of Cy5.5-PTX-SA-CMC NPs for *ex vivo* fluorescence imaging (Fig. 4b). The strongest NIR fluorescence signals was clearly observed in the tumor tissues, indicating that Cy5.5-PTX-SA-CMC NPs were primarily accumulated at the tumor sites. On the contrary, some Cy5.5-PTX-SA-CMC NPs were localized in lung, kidney, and liver. Notably, the mean fluorescence signal in the tumor tissues was 5.0 to 34.2-fold higher compared with that of kidney and heart, respectively (Fig. 4c), which was a further evidence of the passive tumor-targeting ability of PTX-SA-CMC NPs. These results suggested that PTX-SA-CMC NPs showed excellent EPR effect-mediated passive tumor targeting ability in BEL-7402 tumor-bearing mice, which could help to efficiently improve the therapeutic efficiency.

3.9. *In vivo* antitumor efficiency of PTX-SA-CMC NPs (14.9 wt%)

To explain the *in vivo* antitumor efficiency of PTX-SA-CMC NPs, the BEL-7402 liver tumor-bearing Kunming mice were treated with Cremophor EL-based PTX and PTX-SA-CMC NPs (14.9 wt%). These formulations at PTX concentration of 20 mg/kg (was the maximum tolerated dose) [43] were intravenously injected into mice through the vein tail at 0, 4, and 8 d (Fig. 4d). As controls, 200 μL of empty SA-CMC NPs (115 mg/kg) or physiological saline were also administrated into mice. At the end of the antitumor research, the SA-CMC NPs (without PTX) therapy produced no obvious tumor growth inhibition compared with physiological saline group. The result indicated that SA-CMC NPs alone had no significant inhibition influence on tumor growth. In addition, when mice were treated with Cremophor-based PTX (20 mg/kg) or PTX-SA-CMC NPs (20 mg/kg), the reduction in tumor growth was much slower. In comparison with the control group, Cremophor EL-based PTX suppressed tumor volume by 48.8% after 35 days. Moreover, PTX-SA-CMC NPs significantly decreased tumor volumes by 73.2%, indicating that the antitumor effect of PTX-SA-CMC NPs was obviously higher compared with that of Cremophor EL-based PTX. This result suggested that the passive targeting effect of PTX-SA-CMC NPs could enhance the accumulation of PTX within the tumor microenvironment and inside the tumor cells, resulting in a more pronounced cytotoxicity.

Next, the *in vivo* survival rate of Cremophor EL-based PTX and PTX-SA-CMC NPs (14.9 wt%) were also examined (Fig. 4e). After injection of physiological saline and empty SA-CMC NPs, all of mice died within 40 days due to the rapid growth of tumors. In addition, the survival rate of mice treated with Cremophor EL-based PTX and PTX-SA-CMC NPs at the equivalent dose of PTX at 20 mg/kg were 30% and 40% at 40 days, respectively. It was deduced that the Cremophor-based PTX exhibited a severe toxicity in tumor-bearing mice. [43] at 50 days, only 10% of mice were still alive when treated with Cremophor EL-based PTX, while was 40% of those were alive after treatment with PTX-SA-CMC NPs. It should be noted that the tumor disappeared completely in three out of 10 mice treated with PTX-SA-CMC NPs at 25 days. It was considered that the increased survival time of mice treated with PTX-SA-CMC NPs was probably due to their better tumor growth inhibition efficacy while decreasing the side effects. These results above suggested that PTX-SA-CMC NPs exhibited more efficient antitumor effect, and simultaneously showed less systemic toxicity in BEL-7402 liver tumor-bearing mice compared with Cremophor EL-based PTX. Therefore, the SA-CMC self-assembled NPs had a potential as a simple, safe, and effective hydrophobic drug carrier for cancer therapy.

4. Conclusion

Taken together, we have successfully designed and synthesized a novel SA-CMC conjugate for the first time. It was found that the amphiphilic SA-CMC conjugate could be self-assembled into NPs, which could stably load the water-insoluble PTX anticancer drug. The most distinctive feature of PTX-SA-CMC NPs as the biocompatible and biodegradable system was their muti-hydrophobic inner cores, which could remarkably accommodate the large amount of PTX. Notably, upon the stimuli of acid, PTX-SA-CMC NPs exhibited the rapid disassembly and accelerated drug release. Besides, cell experiments demonstrated that PTX-SA-CMC NPs had the enhanced cellular uptake effect and cell-killing effect. Moreover, PTX-SA-CMC NPs showed excellent EPR effect-mediated passive tumor targeting ability in BEL-7402 tumor-bearing mice and achieved significant antitumor effect while reducing systemic toxicity. Therefore, it could be expected that the self-assembled SA-CMC NPs had potential applications as a new drug carrier of PTX for cancer chemotherapeutic treatment.

Declaration of competing interest

The authors declare no competing financial interest.

Acknowledgements

This research was financially supported by the National Natural Science Foundation of China (Grant Nos. 81472458, 81773770), the Science and Technology Project of Fujian Province (Grant Nos. 2017R1036-3, 2018R1036-1), the Science and Technology Planning

Project of Xiamen (Grant Nos. 3502Z20154031, 3502Z20163007), the research projects of the Health Commission of Jiangsu Province of China (H2018070), and the “Double-First Class” Foundation of Materials and Intelligent Manufacturing Discipline of Xiamen University.

References

[1] Y. Li, G. Liu, J. Ma, J. Lin, H. Lin, G. Su, et al., Chemotherapeutic drug-photothermal agent co-self-assembling nanoparticles for near-infrared fluorescence and photoacoustic dual-modal imaging-guided chemo-photothermal synergistic therapy, J. Control. Release 258 (2017) 95–107.
[2] G. Zhang, X. Li, Q. Liao, Y. Liu, K. Xi, W. Huang, et al., Water-dispersible PEG-curcumin/amine-functionalized covalent organic framework nanocomposites as smart carriers for in vivo drug delivery, Nat. Commun. 9 (2018) 2785.
[3] J. Shi, P.W. Kantoff, R. Wooster, O.C. Farokhzad, Cancer nanomedicine: progress, challenges and opportunities, Nat. Rev. Cancer 17 (2017) 20–37.
[4] Y.M. Zhang, N.Y. Zhang, K. Xiao, Q. Yu, Y. Liu, Photo-controlled reversible microtubule assembly mediated by paclitaxel-modified cyclodextrin, Angew Chem Int Ed Engl 57 (2018) 8649–8653.
[5] D. Wang, C. Yu, L. Xu, L. Shi, G. Tong, J. Wu, et al., Nucleoside analogue-based supramolecular nanodrugs driven by molecular recognition for synergistic cancer therapy, J. Am. Chem. Soc. 140 (2018) 8797–8806.
[6] L. Linderoth, P. Fristrup, M. Hansen, F. Melander, R. Madsen, T.L. Andresen, et al., Mechanistic study of the sPLA2-mediated hydrolysis of a thio-ester pro anticancer ether lipid, J. Am. Chem. Soc. 131 (2009) 12193–12200.
[7] Y. Jin, X. Liang, Y. An, Z. Dai, Microwave-triggered smart drug release from liposomes co-encapsulating doxorubicin and salt for local combined hyperthermia and chemotherapy of cancer, Bioconjug. Chem. 27 (12) (2016) 2931–2942.
[8] M. Delcea, H. Möhwald, A.G. Skirtach, Stimuli-responsive LbL capsules and nanoshells for drug delivery, Adv. Drug Deliv. Rev. 63 (2011) 730–747.
[9] J. Mao, Y. Li, T. Wu, C. Yuan, B. Zeng, Y. Xu, et al., A simple dual-pH responsive prodrug-based polymeric micelles for drug delivery, ACS Appl. Mater. Interfaces 8 (2016) 17109–17117.
[10] K. Liu, X. Jiang, P. Hunziker, Carbohydrate-based amphiphilic nano delivery systems for cancer therapy, Nanoscale 8 (2016) 16091–16156.
[11] A. MaHam, Z. Tang, H. Wu, J. Wang, Y. Lin, Protein-based nanomedicine platforms for drug delivery, Small 5 (2009) 1706–1721.
[12] C. Fante, F. Greco, Polymer-drug conjugates, Fundamentals of Pharmaceutical Nanoscience, 2013, pp. 159–182.
[13] P. Huang, D. Wang, Y. Su, W. Huang, Y. Zhou, D. Cui, et al., Combination of small molecule prodrug and nanodrug delivery: amphiphilic drug–drug conjugate for cancer therapy, J. Am. Chem. Soc. 136 (2014) 11748–11756.
[14] A. Kumar, H. Ma, X. Zhang, K. Huang, S. Jin, J. Liu, et al., Gold nanoparticles functionalized with therapeutic and targeted peptides for cancer treatment, Biomaterials 33 (2012) 1180–1189.
[15] P. Ghosh, G. Han, M. De, C.K. Kim, V.M. Rotello, Gold nanoparticles in delivery applications, Adv. Drug Deliv. Rev. 60 (2008) 1307–1315.
[16] X. Zhang, X. Xu, Y. Li, C. Hu, Z. Zhang, Z. Gu, Virion-like membrane-breaking nanoparticles with tumor-activated cell-and-tissue dual-penetration conquer impermeable cancer, Adv. Mater. 30 (2018) 1707240.
[17] S. Taghavi, A.H. Nia, K. Abnous, M. Ramezani, Polyethylenimine-functionalized carbon nanotubes tagged with AS1411 aptamer for combination gene and drug delivery into human gastric cancer cells, Int. J. Pharm. 516 (2017) 301–312.
[18] C. Sun, L. Wen, J. Zeng, Y. Wang, Q. Sun, L. Deng, et al., One-pot solventless preparation of PEGylated black phosphorus nanoparticles for photoacoustic imaging and photothermal therapy of cancer, Biomaterials 91 (2016) 81–89.
[19] J. Shao, H. Xie, H. Huang, Z. Li, Z. Sun, Y. Xu, et al., Biodegradable black phosphorus-based nanospheres for in vivo photothermal cancer therapy, Nat. Commun. 7 (2016) 12967.
[20] G. Shen, R. Xing, N. Zhang, C. Chen, G. Ma, X. Yan, Interfacial cohesion and assembly of bioadhesive molecules for design of long-term stable hydrophobic nanodrugs toward effective anticancer therapy, ACS Nano 10 (2016) 5720–5729.
[21] J. Shi, P.W. Kantoff, R. Wooster, O.C. Farokhzad, Cancer nanomedicine: progress, challenges and opportunities, Nat. Rev. Cancer 17 (1) (2017) (advance online publication).
[22] D. Peer, J.M. Karp, S. Hong, O.C. Farokhzad, R. Margalit, R. Langer, Nanocarriers as an emerging platform for cancer therapy, Nat. Nanotechnol. 2 (2007) 751–760.
[23] S. Wilhelm, A.J. Tavares, Q. Dai, S. Ohta, J. Audet, H.F. Dvorak, et al., Analysis of nanoparticle delivery to tumours, Nat Rev Mater 1 (2016) 16014.
[24] Q. Pei, X. Hu, S. Liu, Y. Li, Z. Xie, X. Jing, Paclitaxel dimers assembling nanomedicines for treatment of cervix carcinoma, J. Control. Release 254 (2017) 23–33.
[25] E.K. Rowinsky, R.C. Donehower, Paclitaxel (Taxol), N. Engl. J. Med. 332 (1995) 1004–1014.
[26] H. Gelderblom, J. Verweij, K. Nooter, A. Sparreboom, Cremophor EL: the drawbacks and advantages of vehicle selection for drug formulation, Eur. J. Cancer 37 (2001) 1590–1598.
[27] J.P. Nam, J.W. Nah, Target gene delivery from targeting ligand conjugated chitosan-PEI copolymer for cancer therapy, Carbohydr. Polym. 135 (2016) 153–161.
[28] J.H. Lee, A. Sahu, W.I. Choi, J.Y. Lee, G. Tae, ZOT-derived peptide and chitosan functionalized nanocarrier for oral delivery of protein drug, Biomaterials 103 (2016) 160–169.
[29] Y. Su, Y. Hu, Y. Du, X. Huang, J. He, J. You, et al., Redox-responsive polymer-drug conjugates based on doxorubicin and chitosan oligosaccharide-g-stearic acid for cancer therapy, Mol. Pharm. 12 (2015) 1193–1202.
[30] Z.L. Peng, S.H. Li, X. Han, A.O. Al-Youbi, A.S. Bashammakh, M.S. El-Shahawi, et al., Determination of the composition, encapsulation efficiency and loading capacity in protein drug delivery systems using circular dichroism spectroscopy, Anal. Chim. Acta 937 (2016) 113–118.
[31] T. Baran, A. Menteş, H. Arslan, Synthesis and characterization of water soluble O-carboxymethyl chitosan Schiff bases and Cu(II) complexes, Int. J. Biol. Macromol. 72 (2015) 94–103.
[32] T. Baran, A. Menteş, Cu(II) and Pd(II) complexes of water soluble O-carboxymethyl chitosan Schiff bases: synthesis, characterization, Int. J. Biol. Macromol. 79 (2015) 542–554.
[33] K. Kalyanasundaram, J.K. Thomas, Environmental effects on vibronic band intensities in pyrene monomer fluorescence and their application in studies of micellar systems, J. Am. Chem. Soc. 99 (1977) 2039–2044.
[34] K.Y. Lee, W.H. Jo, I.C. Kwon, Y.-H. Kim, S.Y. Jeong, Physicochemical characteristics of self-aggregates of hydrophobically modified chitosans, Langmuir: The ACS Journal of Surfaces and Colloids 14 (1998) 2329–2332.
[35] A. R, W. BC, Effect of pH on the critical micelle concentration of sodium dodecyl sulphate, J. Appl. Polym. Sci. 28 (1983) 1331–1334.
[36] Y.-S. Wang, L.-R. Liu, Q. Jiang, Q.-Q. Zhang, Self-aggregated nanoparticles of cholesterol-modified chitosan conjugate as a novel carrier of epirubicin, Eur. Polym. J. 43 (2007) 43–51.
[37] K. Akiyoshi, S. Deguchi, H. Tajima, T. Nishikawa, J. Sunamoto, Microscopic structure and thermoresponsiveness of a hydrogel nanoparticle by self-assembly of a hydrophobized polysaccharide, Macromolecules 30 (1997) 857–861.
[38] E. Blanco, H. Shen, M. Ferrari, Principles of nanoparticle design for overcoming biological barriers to drug delivery, Nat. Biotech. 33 (2015) 941–951.
[39] J.-H. Kim, Y.-S. Kim, S. Kim, J.H. Park, K. Kim, K. Choi, et al., Hydrophobically modified glycol chitosan nanoparticles as carriers for paclitaxel, J. Control. Release 111 (2006) 228–234.
[40] J. You, F.Q. Hu, Y.Z. Du, H. Yuan, B.F. Ye, High cytotoxicity and resistant-cell reversal of novel paclitaxel loaded micelles by enhancing the molecular-target delivery of the drug, Nanotechnology 18 (2007) 495101.
[41] M. Chen, Y. Liu, W. Yang, X. Li, L. Liu, Z. Zhou, et al., Preparation and characterization of self-assembled nanoparticles of 6-O-cholesterol-modified chitosan for drug delivery, Carbohydr. Polym. 84 (2011) 1244–1251.
[42] F.Q. Hu, G.F. Ren, H. Yuan, Y.Z. Du, S. Zeng, Shell cross-linked stearic acid grafted chitosan oligosaccharide self-aggregated micelles for controlled release of paclitaxel, Colloids Surf. B: Biointerfaces 50 (2006) 97–103.
[43] S.C. Kim, D.W. Kim, Y.H. Shim, J.S. Bang, H.S. Oh, S. Wan Kim, et al., In vivo evaluation of polymeric micellar paclitaxel formulation: toxicity and efficacy, Journal of Controlled Release: Official Journal of the Controlled Release Society 72 (2001) 191–202.